Dyes and Pigments 89 (2011) 284–289

Contents lists available at ScienceDirect

Dyes and Pigments

journal homepage: www.elsevier.com/locate/dyepig

A dihydroindolizine-porphyrin dyad as molecule-based all-photonic AND and NAND gates

Joakim Andréasson [a,*], Yuichi Terazono [b], Mattias P. Eng [a], Ana L. Moore [b], Thomas A. Moore [b], Devens Gust [b]

[a] Department of Chemical and Biological Engineering, Physical Chemistry, Chalmers University of Technology, SE-412 96 Göteborg, Sweden
[b] Department of Chemistry and Biochemistry, Arizona State University, Tempe, AZ 85287, USA

ARTICLE INFO

Article history:
Received 23 February 2010
Received in revised form
26 March 2010
Accepted 31 March 2010
Available online 7 April 2010

Keywords:
Chromophores
Molecular devices
Photochemistry
Photochromism
Porphyrinoids
Logic gates

ABSTRACT

A molecular dyad consisting of a photochromic dihydroindolizine unit covalently linked to a porphyrin performs, when illuminated through a third-harmonic-generating crystal, the functions of both an AND and a NAND Boolean logic gate with shared all-optical inputs. The NAND gate is of particular interest as it is a so-called universal gate, and hence all other digital systems can be implemented by combinations of NAND gates. The functions of the AND and the NAND gates rely on changes in absorption and emission of the dyad in the visible spectral region upon isomerization of the photochromic unit. The change in absorption which forms the basis for the AND gate function is ascribed to the colorization/decolorization of the photochrome itself in response to the optical inputs. The variation in emission intensity which constitutes the NAND gate function is a result of the changes in redox properties of the photochrome that follow upon isomerization, such that only one of the two isomers is competent to quench the porphyrin emission by electron transfer.

1. Introduction

Lately, it has been realized that organic molecules can be used as switching elements in Boolean logic constructs [1–7]. Replacing today's silicon-based semiconductor materials with molecular switches would have an enormous impact on information processing and transmission. Typically, the function of the molecular logic constructs reported in the literature relies on the switching of an optically detectable property of the molecule, e.g. changes in absorption or emission [8–34]. In most cases, at least one of the inputs of the logic construct requires physical addition of a chemical species. The material transfer and the diffusion needed for the switching of these constructs impose limitations on the media (fluid solution required) as well as the operational speed, and multiple operation leads to a buildup of byproducts. Molecule-based logic elements with optical inputs and outputs do not require access for chemicals or wires and can in principle operate on a much faster time scale and in rigid or semi-rigid media. Furthermore, using light allows one in principle to use 3-dimensional arrays of volume elements containing the molecules. These can be addressed independently by optical means, using the spatial resolution achieved by focusing the light, two-photon effects, etc., affording higher device densities. Several different kinds of molecular systems, each sensitive to different wavelengths of light, may also be contained within the same diffraction-limited spot. This would increase the device densities even further.

Our main approach to molecule-based logic has been to use photoisomerizable photochromic molecules to constitute the heart of the logic constructs [35]. In addition to a number of simple switches based on photochromic molecules covalently linked to a porphyrin [36–39], we have shown proof of principle for several Boolean logic gates [40–42], a double-throw switch [43], a 2–1 multiplexer [44], a 1–2 demultiplexer [45], two half adders [46,47], an encoder/decoder [48], and a keypad lock [49], all operated using light or heat (which can be supplied by an IR laser) as input and output signals. Here, we report that when illuminated through a third-harmonic-generating crystal, a photochromic dyad (**1**, Scheme 1), consisting of a porphyrin P covalently linked to a dihydroindolizine photochrome DHI, simultaneously performs the functions of both an AND gate and a NAND gate, operated with light as inputs and outputs.

The NAND gate, together with the NOR gate, is a so-called *universal* gate, as any digital system can be implemented by combinations of NAND gates [50]. Therefore, NAND gates typically form the basis of all other logic hardware. Following the first

* Corresponding author. Tel.: +46 31 772 2838; fax: +46 31 772 3858.
E-mail address: a-son@chalmers.se (J. Andréasson).

0143-7208/$ – see front matter © 2010 Elsevier Ltd. All rights reserved.
doi:10.1016/j.dyepig.2010.03.033

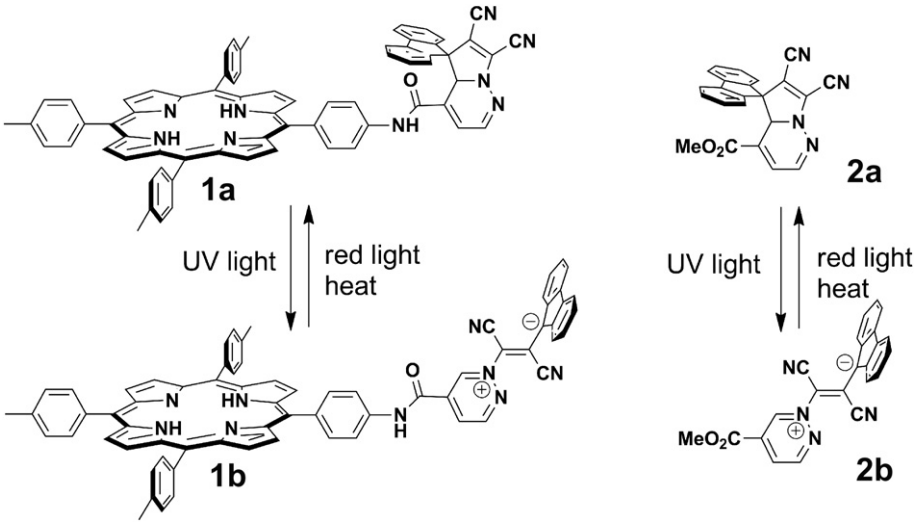

Scheme 1. Structures and isomerization schemes of P-DHI dyad **1** and DHI monomer **2**.

reports on molecular AND [51] and NAND [52] gates, the same functions have been realized by many other groups. In the vast majority of these cases, chemical inputs have been used. The approach used in this work is to make P-DHI dyad **1** perform the desired functions via photoisomerization of the appended DHI photochrome between its two states. The isomerization process induces changes in both the absorption spectrum and the reduction potential of the switching element. In the open, betaine form DHIo of the dyad **1b**, the photochrome displays strong absorption in the visible region. Excitation of the porphyrin is followed by efficient electron transfer to yield $P^{\bullet+}$-$DHIo^{\bullet-}$, and the fluorescence from P is strongly quenched. Visible irradiation of **1b** converts DHIo to the closed, spirocyclic form DHIc, yielding dyad **1a** which absorbs almost exclusively in the UV region. Here, the reduction potential of DHIc is much more negative than that of the open isomer and the energy of the charge separated state increases substantially. Excitation of the porphyrin unit does not lead to any quenching by electron transfer, and the typical emission from P is observed. As discussed below, the observed changes in absorption and emission intensity in the visible region upon switching the state of the DHI photochrome form the basis for the functions of the AND and the NAND gate, respectively.

2. Experimental section

The synthesis and characterization of dyad **1** have been reported [39]. The spectroscopic solvent was distilled 2-methyltetrahydrofuran. The samples were degassed by six freeze-pump-thaw cycles to a final pressure of $\sim 10^{-5}$ Torr.

The absorbance measurements were performed using a CARY 4B UV/Vis spectrometer. For the emission measurements, a SPEX Fluorolog $\tau 2$ was used. The red light used in the reset operation was generated by a 1000 W Xe/Hg-lamp operating at 450 W. The Xe/Hg-lamp light was filtered by two hot mirrors (each having A = 1.8 at 900 nm) to reduce the IR intensity, and a long pass filter (>590 nm) to remove light of shorter wavelengths. The resulting light power density on the sample was $\sim$40 mW/cm^2. The laser used to generate the input signals was a Nd:YAG laser (Continuum Surelight II-10, 6 ns fwhm).

The schematic diagram in Fig. 3 shows all excitation and readout apparatus present in one location. Although such an experimental setup could be assembled in principle, separate instruments already on hand were employed for experimental convenience, as described below.

Outputs X and Y. The readout of output X from dyad **1**, i.e., absorbance at 572 nm, was measured with the absorbance spectrometer described above. The readout of output Y, i.e., the fluorescence intensity at 722 nm, was measured with 590-nm excitation using the spectrofluorimeter described above.

Inputs A and B. For the results shown in Figs. 4–6 and described in the text, only one laser was used to provide both inputs A and B, for reasons of experimental convenience. The schematic diagram in Fig. 3 shows two separate lasers to facilitate the description, and in fact the device could be operated in this configuration. The cuvette containing a solution of dyad **1** ($\sim 0.5 \times 10^{-5}$ M) was irradiated with the Nd:YAG laser described above through SHG and then THG crystals. The wavelength selection was achieved by rotating the crystals into and out of the resonance angle. As a result, the state with input A only on was generated by passing the first harmonic of the laser (1064 nm) through the two non-linear crystals with the SHG crystal tuned off-resonance and the THG crystal tuned in-resonance. The state with input B only on was generated by tuning the SHG crystal in-resonance (532 nm) and the THG crystal off-resonance. When both crystals were in-resonance, 355 nm UV light was generated by the THG crystal. In this configuration, the crystals could not be set completely to 0% harmonic generation. To maximize the degree of discrimination among the isomer populations, a 532 nm dichroic mirror was used to better eliminate the UV light from the 532-nm light (input B *on*), and to eliminate the 532-nm light from the IR light (input A *on*). No filter was used when both inputs were *on*, i.e., when both the SHG and the THG were tuned in-resonance to generate UV light. Had two lasers been available, the use of mirror and crystal tuning could have been avoided. The irradiation powers and times employed were: 1064 nm (300 mW average power at 10 Hz for 35 s), 532 nm (16 mW average power at 10 Hz for 35 s), and 355 nm (11 mW average power at 10 Hz for 35 s).

3. Results and discussion

First, to interpret and understand the results for P-DHI dyad **1**, the previously reported photochemical and photophysical properties will be briefly reviewed. For a more detailed description, please see ref. [39]. Then, the AND gate and the NAND gate functions will be presented. Finally, the long-term performance of the P-DHI dyad

is investigated in terms of its stability toward photobleaching upon repeated photocycling.

3.1. Photochemical properties of dyad *1* and monomer *2*

Dyad **1** consists of a photochromic dihydroindolizine unit covalently linked to a porphyrin. The DHI photochrome is the switching unit of the dyad, and can exist in two different forms. The photoinduced and thermal interconversions between the closed, spirocyclic forms **1a** and **2a** and the open betaine forms **1b** and **2b** are shown in Scheme 1. Fig. 1 shows the absorption spectra of dyad **1** and model monomer **2** in the different forms together with the emission spectra of the porphyrin unit in dyad **1**. The inset shows the absorption spectra of model compound **2a**. This compound absorbs almost exclusively in the UV region, with absorption maxima at 334 and 403 nm. Exposing **2a** to UV light converts it to the open, betaine form **2b**. This compound displays strong absorption in the visible region with bands at 340, 395, and 529 nm. Reversion of **2b**–**2a** results from exposure to visible light or heat. Fig. 1 also shows the absorption of dyad **1a**. Maxima are observed at 419, 483, 515, 550, 593, and 650 nm, where the absorption in the visible region is ascribed to the porphyrin unit of the dyad. UV light exposure isomerizes the dyad to the open form **1b**. The resulting changes in the absorption spectrum are most pronounced between 450 and 650 nm, where the absorption is significantly increased due to isomerization of the DHI photochrome from the closed to the open form. Isomer **1b** reverts slowly thermally to **1a** ($\tau = 182$ min at 20 °C) or faster with visible light.

The isomerization process also causes significant changes in the first reduction potential of the DHI photochrome. In the closed form **2a**, the reduction potential is −1.18 V vs. SCE. For **2b**, the corresponding value is −0.70 V. Hence, **2b** is easier to reduce by almost 0.5 V. The emission spectra from the porphyrin unit of dyads **1a** and **1b** are also shown in Fig. 1. In **1a**, the porphyrin emission displays the typical unperturbed bands at 655 and 722 nm. Isomerization to **1b** results in strong quenching of the emission intensity. The quenching is attributed to photoinduced electron transfer to form $P^{\bullet+}$-DHIo$^{\bullet-}$. The energy of this state is estimated to be 1.68 eV, based on the first reduction potential of **2b** and the first oxidation potential of the porphyrin (0.98 V vs. SCE). As the energy of the lowest excited singlet state of the porphyrin is 1.90 eV, there is a driving force of 0.22 eV for the electron transfer reaction. Energy transfer as the origin of the quenching can be excluded, as such a reaction would be endergonic by ≥0.2 eV [39]. Quenching of the porphyrin emission in **1a** by electron transfer would also be endergonic by 0.26 eV due to the much lower reduction potential of **2a** compared to **2b**.

Time resolved emission studies using the single photon counting technique (SPC) also confirm the efficient quenching of the porphyrin emission in **1b** compared to **1a**. Excitation of a sample of **1a** at 590 nm yields a lifetime for ^{1}P-DHIc of 11.5 ns, which is the typical, unquenched lifetime of a model porphyrin under the conditions used. In **1b**, however, the major decay component has a lifetime of 49 ps, and represents the lifetime of the quenched porphyrin. The dominating deactivation pathways for ^{1}P-DHI in the closed **1a** and the open **1b** forms are summarized in Fig. 2.

Comparing the results from the steady-state emission measurements with the results from the SPC measurements, it is seen that the decrease in emission intensity upon isomerization (ca. 83% quenching efficiency) is smaller than the expected quenching judged by the decrease in lifetime (99.6% quenching efficiency). This is due to the fact that the photostationary distribution after UV exposure at 355 nm is ca. 85/15 **1b**/**1a**. Hence, the major part of the residual emission from the porphyrin after UV exposure is due to unquenched emission from **1a**.

These data demonstrate that light can be used to control both the absorption and the emission intensity of dyad **1** in the visible region. The absorption increases when the sample is exposed to UV light, but decreases when the sample is exposed to visible light or heat. The emission intensity, however, follows the opposite trend; it increases upon exposure to visible light or heat, but decreases upon exposure to UV light. As discussed below, these observations form the basis of the AND gate and the NAND gate, respectively.

3.2. AND gate function

The truth table for an AND gate is shown in Table 1. The gate has two inputs, A and B, and one output, X. The inputs may be either *on* (designated *1*) or *off* (*0*). The AND gate generates an *on* response only when both inputs are *on*. Fig. 3 shows a schematic sketch of how to implement an AND gate based on dyad **1** and a third-harmonic-generating crystal, THG (for convenience, only a single

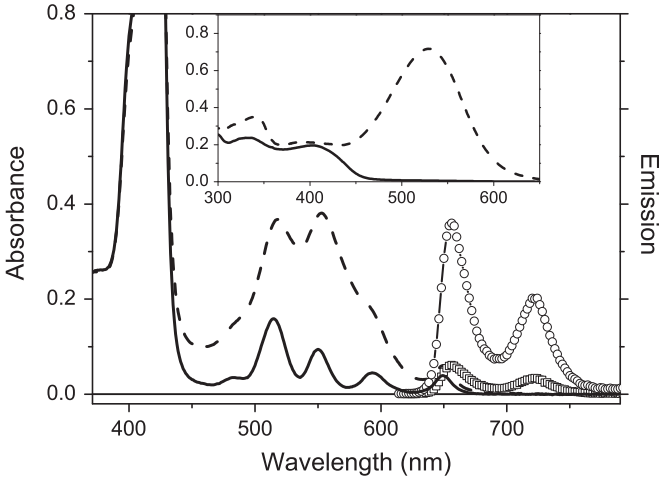

Fig. 1. Absorption spectra of solutions of dyad **1** in the closed **1a** (—) and highly enriched in the open **1b** (– – –) forms. Also shown are the porphyrin emission spectra of these solutions with the dyad in the closed (○–○–○) and highly enriched in the open (□–□–□) forms after excitation at 590 nm. The inset shows the corresponding absorption spectra of the closed **2a** (—) and the open **2b** (– – –) forms of the model monomer.

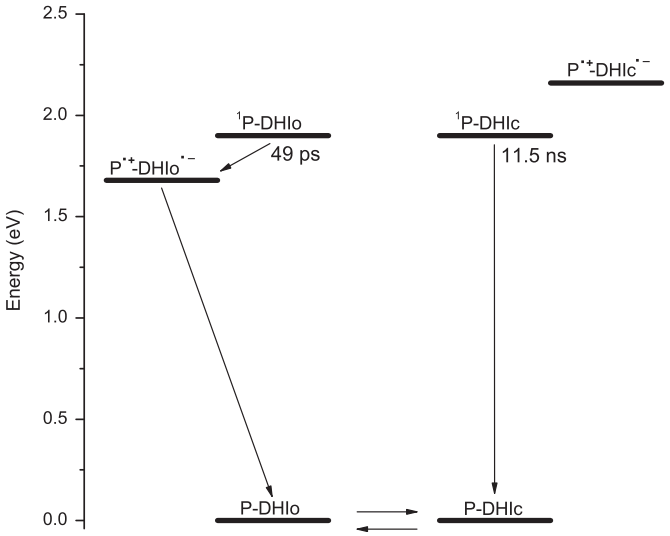

Fig. 2. Transient states and relevant interconversion pathways for dyad **1** with the photochromic moiety in the open, **1o**, form (left) and the closed, **1c**, form (right).

Table 1
Truth table for the AND gate. The choice of input wavelengths is governed by the first and the second harmonics of the Nd:YAG laser.

Input A	Input B	Output X
(1064 nm IR light)	(532 nm visible light)	(Absorbance at 572 nm)
0	0	0
1	0	0
0	1	0
1	1	1

light source was used to provide the two inputs in our experiments, as described in the experimental section). Inputs A and B are defined as 35 s exposure by the first (1064 nm, 10 Hz, 6 ns fwhm, ~300 mW average power) and the second (532 nm, 10 Hz, 6 ns fwhm, ~16 mW average power) harmonics of the Nd:YAG laser, respectively. The output is represented by strong absorption of mainly DHIo in **1b** at 572 nm. In the initial state (after reset), dyad **1** is converted to a photostationary distribution containing mainly the thermally stable **1a** state, P-DHIc. The dyad is set to this state by exposure to red light (~40 mW/cm^2, 590 nm $< \lambda <$ 900 nm) for 2 h. Here, the DHI photochrome is in the closed form, with virtually no absorption at 572 nm. Hence, with neither input *on*, the gate output (strong absorption at 572 nm) is *off*. If input A is applied, no isomerization of P-DHIc to P-DHIo occurs as the dyad is already in the thermally stable form. Hence, the absorbance at 572 nm is still below the threshold level and the gate output remains *off*. Similarly, if input B is applied, only a small portion of the sample is isomerized to the P-DHIo form **1b**. With a proper choice of threshold level, the gate output will still be *off*. Finally, applying both inputs generates 355 nm (~11 mW average power) UV light via the THG. This UV light isomerizes DHIc to DHIo and the dyad is switched from **1a** to **1b**. The absorption of P-DHIo at 572 nm increases above the threshold level and the gate output X is switched *on*. Thus, the molecule meets the criteria for an AND gate, i.e. both inputs must be *on* to switch the output *on*. The actual results from an experiment (absorption of dyad **1** at 572 nm as a function of the different input combinations) are shown in Fig. 4. Before each input combination was applied, the sample was reset to the initial **1a** state by exposure with red light according to above. Please observe that DHIo is not the only absorber at 572 nm. The porphyrin unit displays Q-band absorption in the region between 475 and 675 nm. Hence, the lowest possible absorbance at 572 nm is determined by the Q-band absorption, imposing some limitations on the dynamic range, i.e. the difference between *on* and *off* in the output signal amplitude. It is clear, however, that the dynamic range of the AND gate in Fig. 4 is more than sufficient to distinguish between an *on* and an *off* value. Another important parameter that determines the

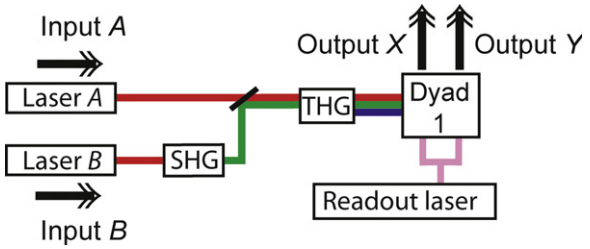

Fig. 3. Schematic sketch showing how to implement AND and NAND gate functions using dyad **1** and a third-harmonic-generating crystal (THG). Lasers A and B are pulsed Nd:YAG lasers at 1064 nm. Switching laser B on will produce 532 nm light (via a second-harmonic-generating crystal, SHG). Switching both lasers on simultaneously will produce 355 nm UV light (via the THG). The absorbance at 572 nm (AND gate, output X) and the emission at 722 nm (NAND gate, output Y) of dyad **1** are monitored by a readout laser and suitable diodes for detection.

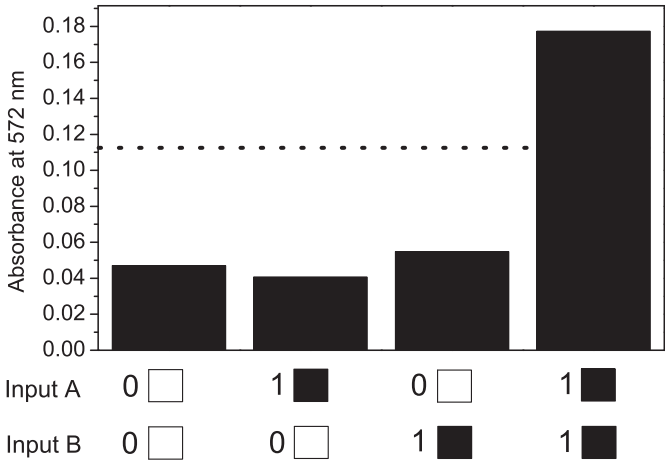

Fig. 4. Performance of dyad **1** in the AND gate mode. The bars show the absorbance measured at 572 nm after each input combination (see text for details). The dotted line represents an arbitrarily set threshold level to distinguish output *on* from output *off*. Before each input combination, the sample was reset to the initial **1a** state using red light.

ability of the gate to distinguish output *on* from output *off* is the associated signal-to-noise of the output signal. Fig. 6a presents the crude output signals measured in a similar cycling experiment, and it is evident that the signals are virtually noise free.

3.3. NAND gate function

The truth table for a NAND gate is shown in Table 2. Similar to the AND gate, the NAND gate also has two inputs, A and B, and one output, here referred to as Y. The NAND gate can be considered as an AND gate followed by an inverter, i.e. the output of a NAND gate is opposite to the output of an AND gate. Consequently, the NAND gate generates an *off* response only when both inputs are *on*. For all other input combinations, the gate output is *on*. Fig. 3 can be used to illustrate also the function of the NAND gate, as both the AND gate and the NAND gate functions are being described by dyad **1** using the same initial state and the same inputs. Accordingly, inputs A and B are 35 s exposure by 1064 nm IR light and 532 nm green light, respectively. Hence, no reconfiguration of the initial state or the input signals is needed for dyad **1** itself to function as two individual logic gates. The output of the NAND gate is strong emission of the porphyrin at 722 nm after excitation at 590 nm. In the initial P-DHIc state **1a**, the DHI unit is in the closed spirocyclic form with relatively low reduction potential. There is no quenching of the porphyrin emission by electron transfer, and the resulting emission intensity is high. Hence, with neither input *on*, the emission intensity is above the threshold level and the gate output is *on*. Applying input A, the IR light will cause no net isomerization to **1b**, the DHI unit is still in the closed form and no electron transfer occurs. The emission intensity is high and the gate output is *on*. Input B will again cause only a small portion of dyad **1** to isomerize to the P-DHIo **1b** form. The emission intensity is still above the

Table 2
Truth table for the NAND gate. The choice of input wavelengths is governed by the first and the second harmonics of the Nd:YAG laser.

Input A	Input B	Output Y
(1064 nm IR light)	(532 nm visible light)	(Emission at 722 nm)
0	0	1
1	0	1
0	1	1
1	1	0

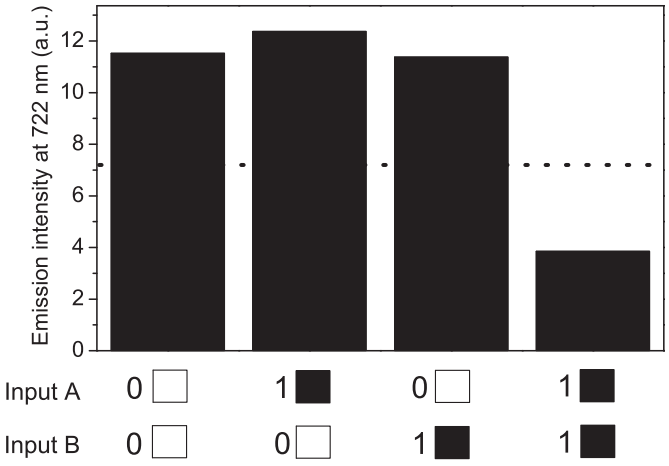

Fig. 5. Performance of dyad **1** in the NAND gate mode. The bars show the emission intensity of the porphyrin unit measured at 722 nm after each input combination (see text for details). The sample was excited at 590 nm. The dotted line represents an arbitrarily set threshold level to distinguish output *on* from output *off*. Before each input combination, the sample was reset to the initial **1a** state.

threshold level and the gate output remains *on*. With both inputs A and B *on*, the resulting 355 nm UV light generated by the THG will isomerize the sample to the open P-DHIo form **1b**. Here, the reduction potential of DHIo is high enough for electron transfer from the porphyrin to occur. The emission of the porphyrin is quenched below the threshold level, and the gate output switches *off*. Thus, the requirements for a NAND gate are met. The experimental results (emission intensity of the porphyrin unit at 722 nm as a function of the different input combinations) are shown in Fig. 5. Before applying each input combination, the sample was reset to the initial **1a** state using red light. The dynamic range for NAND gate operation is virtually identical to that for the AND gate, i.e. output *on* is easily distinguished from output *off*. The associated signal-to-noise of the output signal is presented in Fig. 6b.

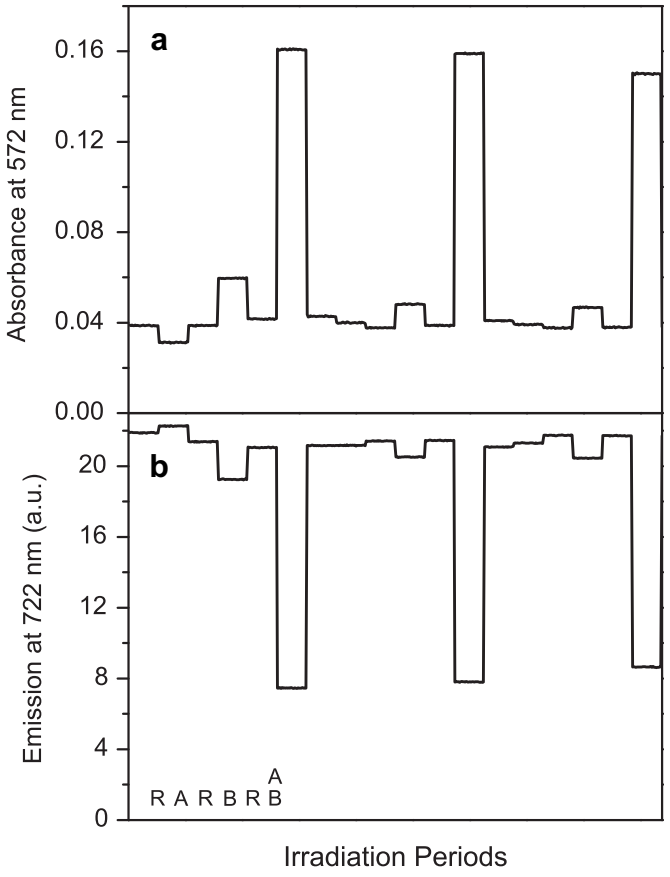

Fig. 6. Photocycling of dyad **1** in the AND gate (a) and the NAND gate mode (b). Both the absorbance and the emission intensity were monitored for 5 s after the input combinations were applied. The associated noise is shown for each measurement. The symbol R indicates the reset operation (2 h red light, 590 nm $< \lambda <$ 900 nm, ~40 mW/cm^2), A indicates input A (35 s 1064 nm pulsed IR light, 10 Hz, 300 mW average power), and B signifies input B (35 s 532 nm pulsed green light, 10 Hz, 16 mW average power). Applying both A and B generates UV light in the THG (35 s 355 nm pulsed UV light, 10 Hz, 11 mW average power).

3.4. Photocycling and photostability

From the experimental results described above, it is obvious that the changes in color and the reduction potential of the photochromic unit of **1** make the dyad mimic the functions of both an AND and a NAND gate, respectively. Although the primary objective of this work has been to show proof of principles rather than producing a practical device, it is still of interest to investigate the fatigue resistance of dyad **1** upon repeated photocycling. It is known that photochromes of the DHI family photo-decompose rapidly in the presence of oxygen [53]. Therefore, the samples were rigorously degassed prior to all experiments by six freeze-pump-thaw cycles to a final pressure of ca. 10^{-5} Torr. The operation of the gate through three cycles is illustrated in Figs. 6a (AND gate mode, absorbance) and 6b (NAND gate mode, emission). The actual signal-to-noise obtained is evident from these data. It is clear that the signals are essentially noise free. Following each measurement, dyad **1** was reset to the initial P-DHIc state using red light and another set of measurements were taken prior to applying the next input combination. Judging from the signal-to-noise ratio and the dynamic range retained after three cycles, it is obvious that the sample can go through several more cycles before it is no longer possible to distinguish between an *off* and an *on* value of the output signal. This is true for both AND and NAND gate operation. It should be noted that the 35 s irradiation doses were selected to yield signals with ample signal-to-noise ratio and minimal sample degradation due to side reactions. They do not achieve the photostationary states of the photochromic DHI moiety and hence, some of each species (DHIc and DHIo) is present in each state of the logic gates. This is another reason for the residual responses of the two gates in the data shown in Figs. 4–6 when the gates are in the *off* state. By choosing suitable threshold values, however, an *on* response is easily distinguished from an *off* response.

4. Conclusions

When illuminated through a third-harmonic-generating crystal, dyad **1** is capable of performing the functions of both an AND and a NAND Boolean logic gate operated by optical inputs and outputs. The dyad performs the AND and the NAND logic operations in parallel, i.e. no reconfiguration of dyad **1** is needed. The output signals of both gates are essentially noise free and based on easily detectable phenomena (absorption and emission) which in principle allows for detection by two separate photodiodes and a light source. The input signals are pulsed laser light at 1064 and 532 nm so that the total irradiation time (with 6 ns pulses) in each input operation was on the order of 2 μs. After each input operation, the gates remember their states for hours and may then be reset to the initial state after readout. Hence, the dyad functions as a storage element of the information contained in the transiently applied

input combinations. The dyad is stable towards photobleaching in degassed solution and may be cycled many times before losing the ability to distinguish between output *on* or *off*. The lower limit for the cycle time of the gates is ultimately determined by the rate of the isomerization reaction, an event that occurs in less than a ns. This is an obvious advantage of light-controlled systems like dyad **1** compared to molecular logic systems that rely on chemical inputs, where the rates of operation are limited by material transfer and diffusional processes.

Acknowledgements

This work was supported by the Swedish Research Council (VR), the European Research Council (grant ERC FP7/2007-2013 No. 203952), and the U.S. National Science Foundation (CHE-0846943).

References

[1] Aviram A. Molecules for memory, logic, and amplification. Journal of the American Chemical Society 1988;110:5687–92.
[2] Ball P. Chemistry meets computing. Nature 2000;406:118–20.
[3] Balzani V, Credi A, Venturi M. Molecular logic circuits. Chemphyschem 2003; 4:49–59.
[4] de Silva AP, Fox DB, Moody TS, Weir SM. Luminescent sensors and photonic switches. Pure and Applied Chemistry 2001;73:503–11.
[5] Andréasson J, Pischel U. Smart molecules at work – mimicking advanced logic operations. Chemical Society Reviews 2010;39:174–88.
[6] Pischel U. Chemical approaches to molecular logic elements for addition and subtraction. Angewandte Chemie International Edition 2007;46:4026–40.
[7] Szaciłowski K. Digital information processing in molecular systems. Chemical Reviews 2008;108:3481–548.
[8] Baron R, Lioubashevski O, Katz E, Niazov T, Willner I. Logic gates and elementary computing by enzymes. Journal of Physical Chemistry A 2006; 110:8548–53.
[9] Credi A, Balzani V, Langford SJ, Stoddart JF. Logic operations at the molecular level. An XOR gate based on a molecular machine. Journal of the American Chemical Society 1997;119:2679–81.
[10] de Silva AP, Leydet Y, Lincheneau C, McClenaghan ND. Chemical approaches to nanometre-scale logic gates. Journal of Physics-Condensed Matter 2006;18: 1847–72.
[11] Fang CJ, Zhu Z, Sun W, Xu CH, Yan CH. New TTF derivatives: several molecular logic gates based on their switchable fluorescent emissions. New Journal of Chemistry 2007;31:580–6.
[12] Gunnlaugsson T, Mac Donaill DA, Parker D. Lanthanide macrocyclic quinolyl conjugates as luminescent molecular-level devices. Journal of the American Chemical Society 2001;123:12866–76.
[13] Guo XF, Zhang DQ, Zhang GX, Zhu DB. Monomolecular logic: "half-adder" based on multistate/multifunctional photochromic spiropyrans. Journal of Physical Chemistry B 2004;108:11942–5.
[14] Langford SJ, Yann T. Molecular logic: a half-subtractor based on tetraphenylporphyrin. Journal of the American Chemical Society 2003;125:11198–9.
[15] Liu Y, Jiang W, Zhang HY, Li CJ. A multifunctional arithmetical processor model integrated inside a single molecule. Journal of Physical Chemistry B 2006; 110:14231–5.
[16] Margulies D, Melman G, Shanzer A. Fluorescein as a model molecular calculator with reset capability. Nature Materials 2005;4:768–71.
[17] Pina F, Melo MJ, Maestri M, Passaniti P, Balzani V. Artificial chemical systems capable of mimicking some elementary properties of neurons. Journal of the American Chemical Society 2000;122:4496–8.
[18] Qu DH, Ji FY, Wang QC, Tian H. A double INHIBIT logic gate employing configuration and fluorescence changes. Advanced Materials 2006;18: 2035–8.
[19] Raymo FM, Giordani S. All-optical processing with molecular switches. Proceedings of the National Academy of Sciences of the United States of America 2002;99:4941–4.
[20] Raymo FM, Giordani S. Multichannel digital transmission in an optical network of communicating molecules. Journal of the American Chemical Society 2002;124:2004–7.
[21] Saghatelian A, Volcker NH, Guckian KM, Lin VSY, Ghadiri MR. DNA-based photonic logic gates: AND, NAND, and INHIBIT. Journal of the American Chemical Society 2003;125:346–7.
[22] Shiraishi Y, Tokitoh Y, Hirai T. A fluorescent molecular logic gate with multiply-configurable dual outputs. Chemical Communications 2005;42:5316–8.
[23] Stojanovic MN, Stefanovic D. Deoxyribozyme-based half-adder. Journal of the American Chemical Society 2003;125:6673–6.
[24] Szacilowski K. Molecular logic gates based on pentacyanoferrate complexes: from simple gates to three-dimensional logic systems. Chemistry – A European Journal 2004;10:2520–8.
[25] Tang YL, He F, Wang S, Li YL, Zhu DB, Bazan GC. Multiply configurable optical-logic systems based on cationic conjugated polymer/DNA assemblies. Advanced Materials 2006;18:2105–10.
[26] Xu H, Xu XH, Dabestani R, Brown GM, Fan L, Patton S, et al. Supramolecular fluorescent probes for the detection of mixed alkali metal ions that mimic the function of integrated logic gates. Journal of the Chemical Society-Perkin Transactions 2 2002;3:636–43.
[27] Zhou YC, Wu H, Qu L, Zhang DQ, Zhu DB. A new redox-resettable molecule-based half-adder with tetrathiafulvalene. Journal of Physical Chemistry B 2006;110:15676–9.
[28] Zong GQ, Xian L, Lu GX. L-Arginine bearing an anthrylmethyl group: fluorescent molecular NAND logic gate with H+ and ATP as inputs. Tetrahedron Letters 2007;48:3891–4.
[29] Ferreira R, Remón P, Pischel U. Multivalued logic with a tristable fluorescent switch. Journal of Physical Chemistry C 2009;113:5805–11.
[30] Margulies D, Felder CE, Melman G, Shanzer A. A molecular keypad lock: a photochemical device capable of authorizing password entries. Journal of the American Chemical Society 2007;129:347–54.
[31] Pérez-Inestrosa E, Montenegro J-M, Collado D, Suau R. A molecular 1: 2 demultiplexer. Chemical Communications; 2008:1085–7.
[32] Remón P, Ferreira R, Montenegro J-M, Suau R, Pérez-Inestrosa E, Pischel U. Reversible molecular logic: a photophysical example of a Feynman gate. ChemPhysChem 2009;10:2004–7.
[33] Silvi S, Constable EC, Housecroft CE, Beves JE, Dunphy EL, Tomasulo M, et al. All-optical integrated logic operations based on chemical communication between molecular switches. Chemistry – A European Journal 2009;15: 178–85.
[34] Ceroni P, Bergamini G, Balzani V. Old molecules, new concepts:$[Ru(bpy)_3]^{2+}$ as a molecular encoder-decoder. Angewandte Chemie International Edition 2009;48:8516–8.
[35] Gust D, Moore TA, Moore AL. Molecular switches controlled by light. Chemical Communications; 2006:1169–78.
[36] Bahr JL, Kodis G, de la Garza L, Lin S, Moore AL, Moore TA, et al. Photoswitched singlet energy transfer in a porphyrin-spiropyran dyad. Journal of the American Chemical Society 2001;123:7124–33.
[37] Liddell PA, Kodis G, Andréasson J, de la Garza L, Bandyopadhyay S, Mitchell RH, et al. Photonic switching of photoinduced electron transfer in a dihydropyrene-porphyrin-fullerene molecular triad. Journal of the American Chemical Society 2004;126:4803–11.
[38] Liddell PA, Kodis G, Moore AL, Moore TA, Gust D. Photonic switching of photoinduced electron transfer in a dithienylethene-porphyrin-fullerene triad molecule. Journal of the American Chemical Society 2002;124:7668–9.
[39] Terazono Y, Kodis G, Andréasson J, Jeong GJ, Brune A, Hartmann T, et al. Photonic control of photoinduced electron transfer via switching of redox potentials in a photochromic moiety. Journal of Physical Chemistry B 2004; 108:1812–4.
[40] Andréasson J, Terazono Y, Albinsson B, Moore TA, Moore AL, Gust D. Molecular AND logic gate based on electric dichroism of a photochromic dihydroindolizine. Angewandte Chemie International Edition 2005;44:7591–4.
[41] Straight SD, Andréasson J, Kodis G, Bandyopadhyay S, Mitchell RH, Moore TA, et al. Molecular AND and INHIBIT gates based on control of porphyrin fluorescence by photochromes. Journal of the American Chemical Society 2005; 127:9403–9.
[42] Straight SD, Liddell PA, Terazono Y, Moore TA, Moore AL, Gust D. All-photonic molecular XOR and NOR logic gates based on photochemical control of fluorescence in a fulgimide-porphyrin-dithienylethene triad. Advanced Functional Materials 2007;17:777–85.
[43] Straight SD, Andréasson J, Kodis G, Moore AL, Moore TA, Gust D. Photochromic control of photoinduced electron transfer. Molecular double-throw switch. Journal of the American Chemical Society 2005;127:2717–24.
[44] Andréasson J, Straight SD, Bandyopadhyay S, Mitchell RH, Moore TA, Moore AL, et al. Molecular 2: 1 digital multiplexer. Angewandte Chemie International Edition 2007;46:958–61.
[45] Andréasson J, Straight SD, Bandyopadhyay S, Mitchell RH, Moore TA, Moore AL, et al. A molecule-based 1: 2 digital demultiplexer. Journal of Physical Chemistry C 2007;111:14274–8.
[46] Andréasson J, Kodis G, Terazono Y, Liddell PA, Bandyopadhyay S, Mitchell RH, et al. Molecule-based photonically switched half-adder. Journal of the American Chemical Society 2004;126:15926–7.
[47] Andréasson J, Straight SD, Kodis G, Park CD, Hambourger M, Gervaldo M, et al. All-photonic molecular half-adder. Journal of the American Chemical Society 2006;128:16259–65.
[48] Andréasson J, Straight SD, Moore TA, Moore AL, Gust D. Molecular all-photonic encoder-decoder. Journal of the American Chemical Society 2008;130: 11122–8.
[49] Andréasson J, Straight SD, Moore TA, Moore AL, Gust D. An all-photonic molecular keypad lock. Chemistry – A European Journal 2009;15:3936–9.
[50] Mano MM, Ciletti MD. Digital design. 4th ed. Upper Saddle River, NJ: Pearson Education Inc; 2007.
[51] de Silva AP, Gunaratne HQN, McCoy CP. A molecular photoionic AND gate based on fluorescent signalling. Nature 1993;364:42–4.
[52] Baytekin HT, Akkaya EU. A molecular NAND gate based on Watson–Crick base pairing. Organic Letters 2000;2:1725–7.
[53] Dürr H, Gross H, Agfa-Gevaert NV. Netherlands Research Disclosure 1981;205:188–90.